Basin Research (2007) **19**, 437–450, doi: 10.1111/j.1365-2117.2007.00328.x

Geometry of half-grabens containing a mid-level viscous décollement

Ruth Soto,* Antonio M. Casas-Sainz† and Pedro del Río‡

*Dpto. Física, Univ. Burgos, Av. Cantabria s/n, Burgos, Spain
†Dpto. Ciencias de la Tierra, Univ. Zaragoza, C/Pedro Cerbuna, Zaragoza, Spain
‡Fac. Ciencias del Mar y Ambientales, Universidad de Cádiz, Cádiz, Spain

ABSTRACT

In this work, we explore by means of analogue models how different basin-bounding fault geometries and thickness of a viscous layer within the otherwise brittle pre-rift sequence influence the deformation and sedimentary patterns of basins related to extension. The experimental device consists of a rigid wooden basement in the footwall to simulate a listric fault. The hangingwall consists of a sequence of pre-rift deposits, including the shallow interlayered viscous layer, and a syn-rift sequence deposited at constant intervals during extension. Two different geometries exist of listric normal faults, dip at 30 and 60° at surface. This imposes different geometries in the hangingwall anticlines and their associated sedimentary basins. A strong contrast exists between models with and without a viscous layer. With a viscous décollement, areas near the main basement fault show a wide normal drag and the hangingwall basin is gently synclinal, with dips in the fault side progressively shallowing upwards. A secondary roll-over structure appears in some of the models. Other structures are: (1) reverse faults dipping steeply towards the main fault, (2) antithetic faults in the footwall, appearing only in models with the 30° dipping fault and silicone-level thicknesses of 1 and 1.5 cm and (3) listric normal faults linked to the termination of the detachment level opposite to the main fault, with significant thickness changes in the syn-tectonic units. The experiments demonstrate the importance of detachment level in conditioning the geometry of extensional sedimentary basins and the possibility of syncline basin geometries associated with a main basement fault. Comparison with several basins with half-graben geometries containing a mid-level décollement supports the experimental results and constrains their interpretation.

INTRODUCTION

The presence of ductile detachment layers (i.e. evaporites and overpressured shales) within the pre-tectonic sequence is considered to be an important factor controlling the geometry and kinematics of deformation on compressional (e.g. Pyrenees, Betic Chain, Zagros, Jura) (Phillippe *et al*., 1998; Sans & Koyi, 2001; Costa & Vendeville, 2002; Luján *et al*., 2003; Bahroudi & Koyi, 2004), extensional (e.g. Santos basin, Gulf of Mexico basin, Gulf of Suez, North Sea Rift System, Danish Central Graben, Iberian Chain) (Nalpas & Brun, 1993; Vendeville *et al*., 1995; Ge *et al*., 1997; Withjack & Callaway, 2000; Cartwright *et al*., 2001; Rank-Friend & Elders, 2004; Rodríguez-López *et al*., in press) and strike–slip regimes (e.g. Rhine–Bresse transfer zone) (Richard, 1991; Ustaszewski *et al*., 2005). Specifically, in extensional scenarios, many works have addressed the role of salt in modifying the syn-rift fills during the main phase of rifting, as in the case of the Zechstein salt on the Mesozoic North Sea rift system and Central Graben (e.g. Coward & Stewart, 1995; Clark *et al*., 1998; Rank-Friend & Elders, 2004).

The geometry of the sedimentary filling of extensional basins is conditioned by: (1) the geometry of the normal faults limiting the basin (e.g. McClay & Ellis, 1987a, b; Ellis & McClay, 1988), (2) the amount of extension and deformation rate (e.g. Withjack & Callaway, 2000) and (3) the thickness and rheology of the viscous layer and cover sequence (e.g. Vendeville *et al*., 1987; Nalpas & Brun, 1993; Withjack & Callaway, 2000). In this work, we use scaled analogue models to study the deformation pattern, the subsurface geometry and the syn-sedimentary features linked to the formation of half-grabens with an interlayered décollement (i.e. viscous layer) within the pre-rift sequence.

The objectives of this work are to characterize the structures formed in extensional half-grabens and to give clues (variations of bed thickness and dip changes along the filling of the basin) to identify features related to graben formation, even after processes of basin inversion. A comparison with natural examples supports the experimental device. Furthermore, the results obtained provide new tools to interpret the geometry of basins, as it is the case of the Cameros basin (North Spain), a good example of an

Correspondence: Ruth Soto, Dpto. Física, Univ. Burgos, Av. Cantabria s/n, 09006 Burgos, Spain. E-mail: rlsoto@ubu.es

inverted sedimentary basin formed over a shallow detachment level (Upper Triassic evaporites). The experimental results indicate that a viscous layer in the pre-rift deposits plays a major role in controlling the geometry and deformation of sedimentary basins. Our work implies that in the reconstruction of the extensional geometry of sedimentary basins, it is fundamental to know whether viscous layers are present in the sedimentary pile, and their thickness relative to the pre- and syn-rift sequences. This is especially important when no subsurface data (i.e. seismic profiles) are available, or when the basin has been inverted.

EXPERIMENTAL METHOD

The experiments were carried out in a glass-walled deformation rig 80 cm long × 30 cm wide × 30 cm high. A rigid footwall block with a normal fault, listric geometry was attached to the fixed end wall (Fig. 1). A mylar sheet attached to the outside of the other (moving) end wall initially ended at the tip of the listric fault (i.e. footwall cut-off during the experiments) (Fig. 1), and pulled apart with a constant displacement rate (see Table 1). This arrangement produced extensional displacement on the hangingwall, consisting of a sand–silicone stratified system. The footwall was also covered with a mylar sheet to ensure identical frictional properties during extension. Pre-rift and syn-rift sediments were deposited both over the hangingwall and footwall, except for model 60A, where sand simulating the syn-rift sequence was only deposited on the hangingwall. Pre-rift layers of alternating white and coloured sand (100–300 μm in size and $\varphi = 33.5^\circ$ internal friction angle measured in the laboratory) were sieved and arranged into a horizontal sequence 125 mm thick. In the brittle–ductile models, an interlayered level of silicone within the pre-rift sediments, overlying both the hangingwall and the rigid footwall, acted as a shallow viscous detachment level. The silicone putty used is Rhodorsil Gomme FB of Rhodia silicones. It is a nearly Newtonian fluid with a density of 0.97 g cm^{-3} and a viscosity of 1×10^4 Pa · s at room temperature for the displacement rate used during the experiments (1.5–6 cm h^{-1}). The viscosity was measured with a concentric-cylinder viscometer (see Weijermars, 1986) in the University of Zaragoza. Finally, a thin cover of sand, simulating the top of the pre-rift, was deposited on top of the silicone level.

During extension, white and coloured sand layers, representing the syn-rift sedimentary sequence were added after every 15 mm of displacement of the moving wall. Total extension was 125 mm for most of the models. Once the models were finished, they were impregnated with water and serially sectioned and photographed to analyse their geometrical features. Only the central sections were used to define their geometry to avoid boundary effects. Because the evolution of models cannot be determined from observation of the walls, a series of models with different displacement rates were constructed to record the deformation history.

Models simulated the effect of two principal variables (Table 1): (1) the geometry of the listric fault and (2) the thickness of the shallow interlayered décollement. Listric normal faults dipped at the surface at 30° (gently curved) and 60° (sharply curved). The initial thickness of the ductile level was 0, 5, 10 and 15 mm in the different experimental series.

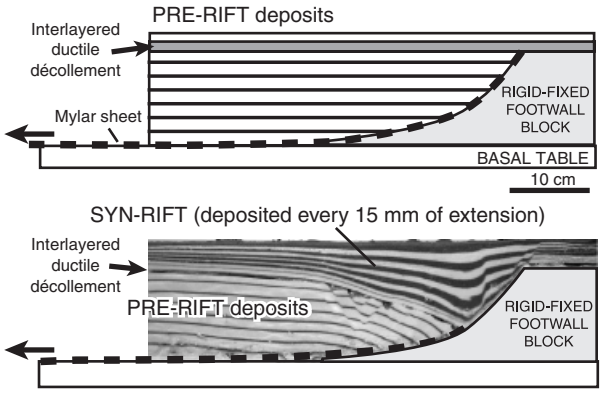

Fig. 1. Experimental apparatus used in this work.

Table 1. Initial configuration of experiments

Model	Master fault (dip angle at surface) (°)	Displacement rate (cm h^{-1})	Viscous layer thickness (mm)	Time (h)
30A	30	6	0	3.25
30B	30	1.5	5	10
30C	30	1.5	10	10
30D	30	1.5	15	10
60A	60	6	0	3.25
60B	60	1.5	5	10
60C	60	1.5	10	10
60D	60	1.5	15	10
60E	60	1.5	10	2
60F	60	1.5	10	4
60G	60	1.5	10	6
60H	60	1.5	10	8

RESULTS

The evolution of models analysing the hangingwall extensional geometry above major listric faults and linked to the formation of half-grabens has been widely described (e.g. McClay & Ellis, 1987a, b; Ellis & McClay, 1988; McClay, 1989; Buchanan & McClay, 1991). Specifically, Ellis & McClay (1988) studied in detail the influence of the geometry of the listric extensional faults on the hangingwall deformation. Withjack & Callaway (2000) studied in detail the influence of a shallow décollement associated with slip of a single fault. However, the influence of shallow viscous décollements within the pre-rift deposits on the hangingwall deformation above listric faults at the basin scale has not yet been studied. Two experiments (models 30A and 60A) were performed without a viscous layer as reference models.

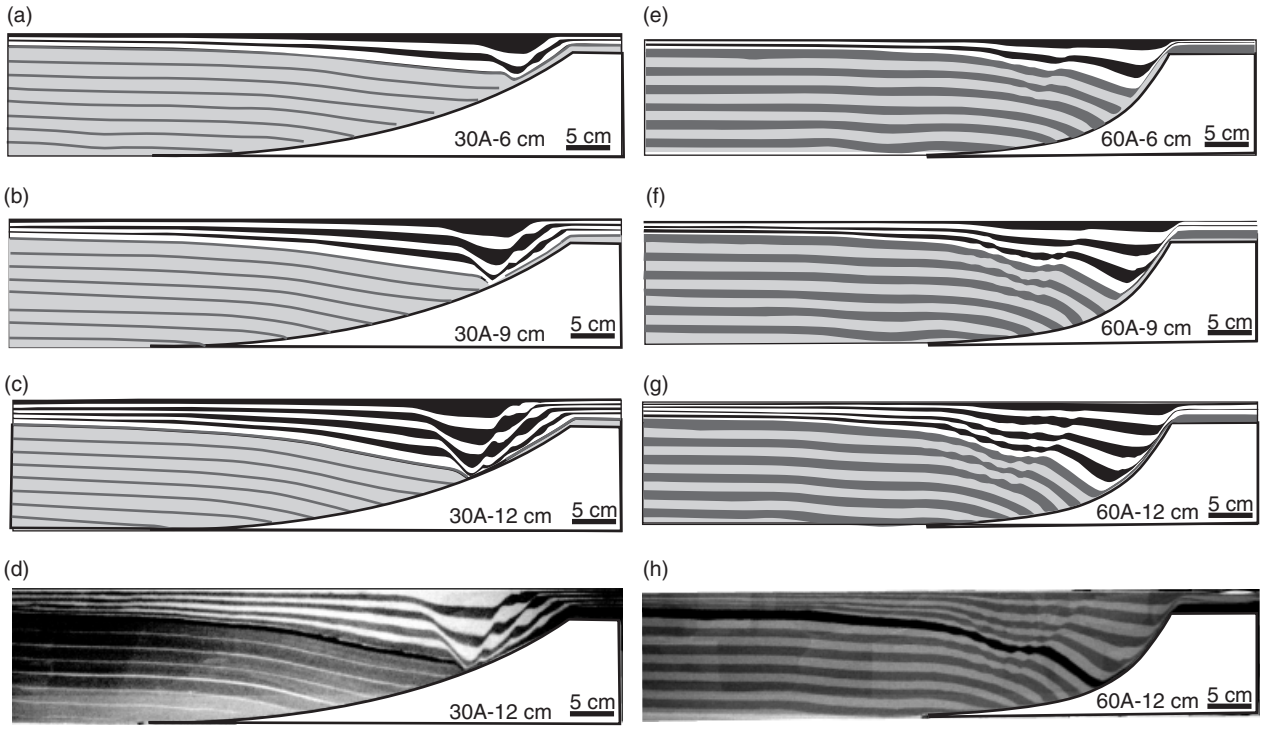

Fig. 2. Line drawings (from cross-section photographs) illustrating the evolution of models 30A and 60A after (a, e) 6 cm, (b, f) 9 cm and (c, g) 12 cm of extension. (d, h) Cross-section photographs of models 30A and 60A after 12 cm of extension.

Brittle models. Influence of listric fault geometry

In models without an interlayered viscous layer, a roll-over anticline formed in the pre-rift hangingwall, its width increasing with decreasing curvature of the listric fault (Fig. 2). Synchronous crestal-collapse faults (synthetic and antithetic with respect to the master fault) formed on the roll-over anticline. This fault system is much more important in the model with higher curvature of the basal listric fault (model 60A) (Fig. 2). The crestal-collapse faults propagated upward through the syn-rift sequence during extension. This propagation was also more important in the model with the more highly curved listric fault (Fig. 2).

Syn-rift geometry also depended strongly on the curvature of the listric fault. In both the 30A and 60A models, the extensional basin was a half-graben with strong thickness variations of the syn-rift deposits near the listric normal fault, where deformation also concentrated (Fig. 2). In the two models, the syn-rift layers were rotated around horizontal axes to accommodate extension in the hangingwall, this rotation being higher in model 60A (Fig. 2). The upward-propagating crestal-collapse faults from the roll-over pre-rift deposits were the only faults in model 60A. Close to the major listric fault, the syn-rift layers reached maximum thickness (Fig. 2). In model 30A, an array of subparallel and synthetic listric faults developed with 65° of dip angle in the syn-rift deposits close to the major listric fault. These normal faults nucleated at the hangingwall cut-off of the pre-rift layers. Whereas the pre-rift sequence accommodated extension by means of a roll-over anticline, in the syn-rift deposits these normal faults nucleated following a hangingwall sequence and propagating towards the basin centre during deformation. A single, antithetic 60°-dip normal fault associated with them at the opposite margin of the fault system also migrated inward. The conjugate normal fault system conditioned the position of the depocentre of the basin that consequently also migrates towards the basin centre during extension (Fig. 2). Our results confirm that the geometry of the basin and the location of the depocentre are strongly conditioned by the geometry of the marginal major listric fault.

Brittle–ductile models. Influence of a shallow interlayered décollement

The pre-rift sequence in brittle–ductile experiments defined a roll-over anticline whose geometry depended on the shape of the listric normal fault (narrower anticline with a higher dip angle at the surface of the listric fault), as in the brittle models. However, the geometry of the pre-rift sequence below the detachment level was not influenced by the presence of the viscous detachment (Fig. 3).

The first difference in the brittle–ductile models was that the viscous layer inhibited the upward propagation of the crestal-collapse faults through the syn-rift sequence and the pre-rift layer located above the detachment level (Figs 3 and 4). The syn-rift deposits of all brittle–ductile models described a growth syncline (Fig. 3). The syn-rift

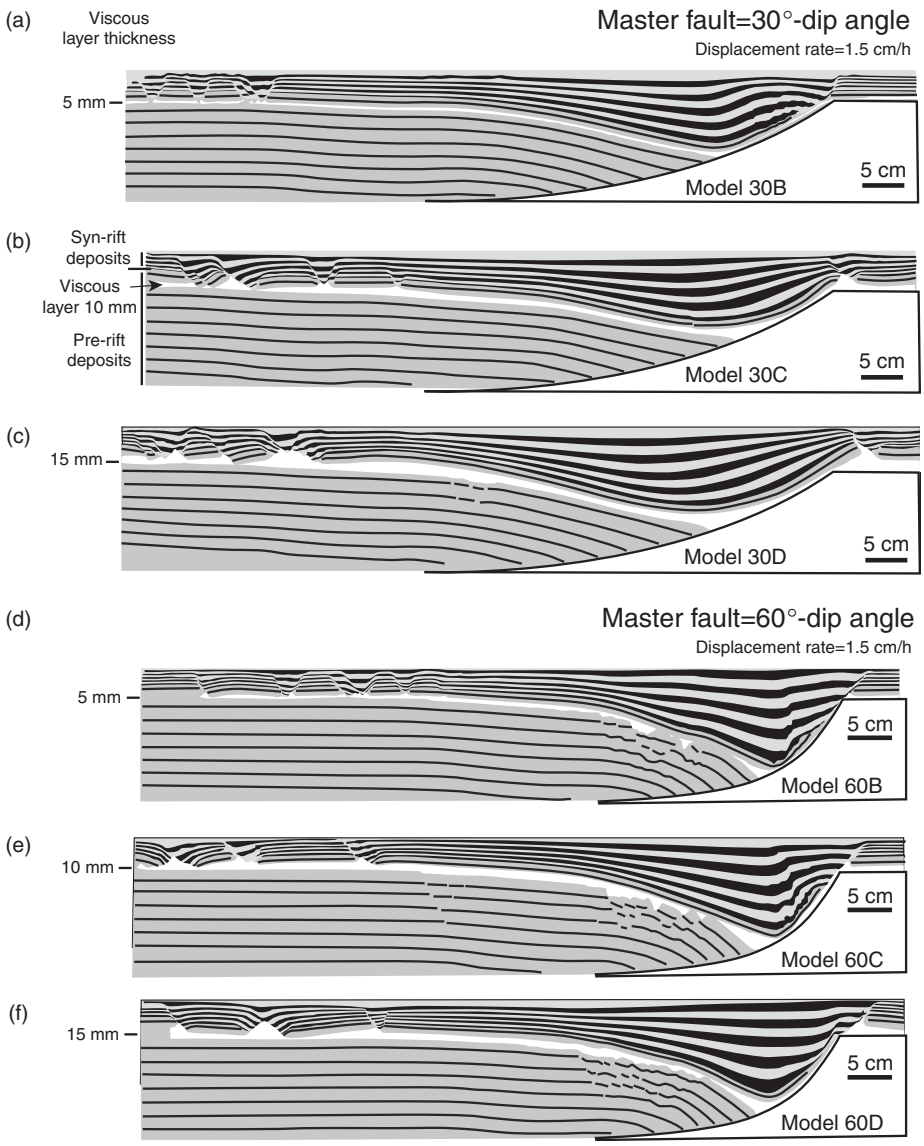

Fig. 3. Line drawings (from cross-section photographs) illustrating the final stage of models (a, b and c) 30B, 30C and 30D, and (d, e and f) 60B, 60C and 60D.

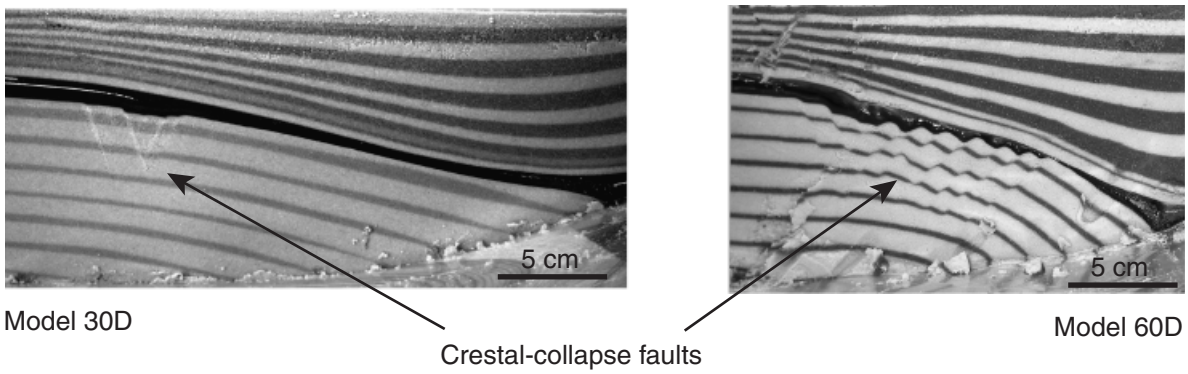

Fig. 4. Photographs of models 30D and 60D (i.e. similar viscous layer thickness) showing the crestal-collapse faults associated with the roll-over anticline of the pre-rift sequence. Note that the viscous layer inhibited the upward propagation of these faults through the syn-rift sequence.

layers near the major fault showed increasing dips as the major fault surface steepened (Fig. 3). Experiments with a thinner ductile level (models 30B and 60B) and model 60C displayed a secondary roll-over anticline near the bounding fault that produced thickness variations of the syn-rift deposits (Figs 3 and 5). This structure was narrower in models with steeper listric fault surface, where also associated reverse faults developed in the back flank of this

anticline (Fig. 5). Conversely, in model 30B, a series of normal faults cut across this secondary roll-over (Fig. 5). In all experiments, except model 30B, reactive salt walls (Vendeville & Jackson, 1992) appeared in the overburden near the footwall cut-off of the listric normal fault (Figs 3 and 6). The size of the salt walls depended on the thickness of the viscous layer (higher with thicker viscous layer) and the geometry of the major listric fault (higher with 30°-dipping fault) (Figs 3 and 6). In 60°-dipping fault models, the salt walls were smaller due to a faster and higher thinning of the viscous layer on the steeper fault plane. In models with a shallower dip angle of the master fault (models 30B and 30C), an antithetic normal fault appeared in the footwall of the master fault, associated with the salt walls (Figs 3 and 6). In the rest of the models, a normal fault, synthetic with the main basement fault, nucleated in an equivalent position.

The viscous detachment thinned considerably over the master fault and thickened at the hangingwall cut-off of the pre-rift sequence in all models (Figs 3 and 6). Contrasting with the brittle models, in brittle-ductile models listric faults formed in the syn-rift sequence, at the end of the model opposite to the main fault and linked to the termination of the detachment level (Figs 3 and 7). Most faults of this system were antithetic with respect to the main fault. They were associated with reactive diapirs (mostly salt rollers) and overlying syn-rift half-grabens and grabens (Figs 3 and 7). The characteristic viscous structures related to this fault system were salt rollers and salt walls, associated with the new-formed listric faults and salt welds at the base, linked to the migration of the viscous layer (Fig. 7).

These fault systems near the end of the detachment level accommodated large horizontal extension in some models (Fig. 8). This strongly contrasts with the brittle models, where deformation was concentrated near the main fault. The extension of this fault system is related to the thickness of the detachment level: a thicker viscous layer allowed more extension (Fig. 8).

Our experimental results, described above, indicate that the introduction of a viscous interlayered level largely influences the geometry of the basin. Thickness variations of the viscous layer also control its sedimentary architecture.

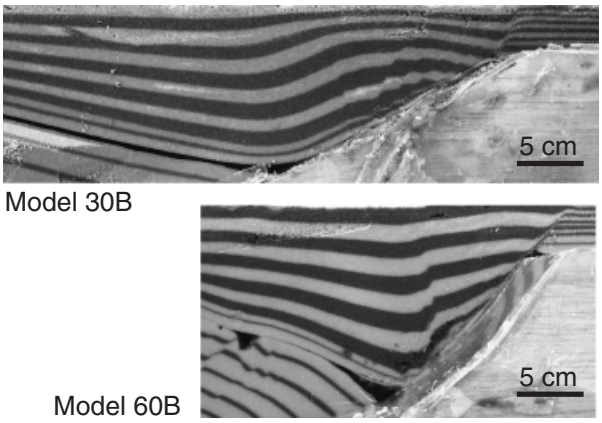

Fig. 5. Photographs of models 30B and 60B (i.e. similar viscous layer thickness) illustrating the secondary roll-over anticline of the syn-rift deposits. Normal faults cross this structure in model 30B, whereas associated reverse faults characterize model 60B.

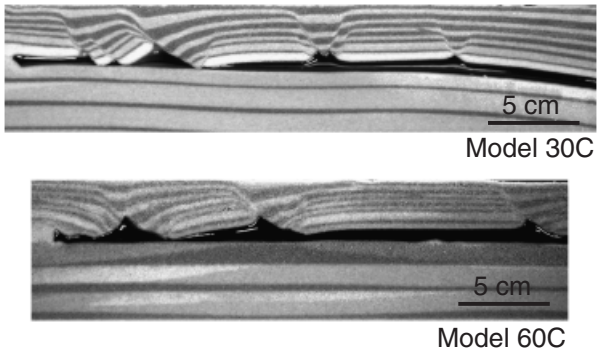

Fig. 7. Photographs of models 30C and 60C (i.e. similar viscous layer thickness) showing the fault system linked to the termination of the viscous layer at the opposite margin of the basin.

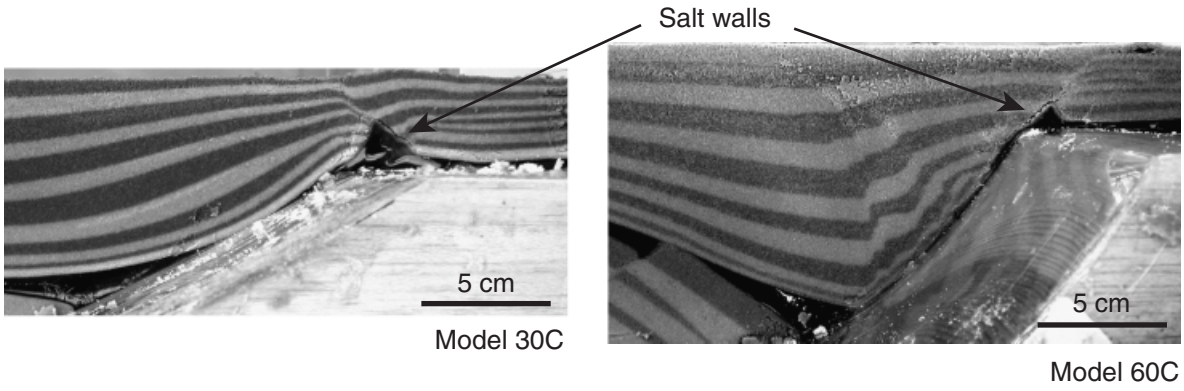

Fig. 6. Photographs of models 30C and 60C (i.e. similar viscous layer thickness) showing the salt walls formed at the footwall cut-off and associated antithetic and normal fault, respectively. Note the strong thinning over the master fault and thickening at the hangingwall cut-off of the pre-rift sequence of the viscous layer.

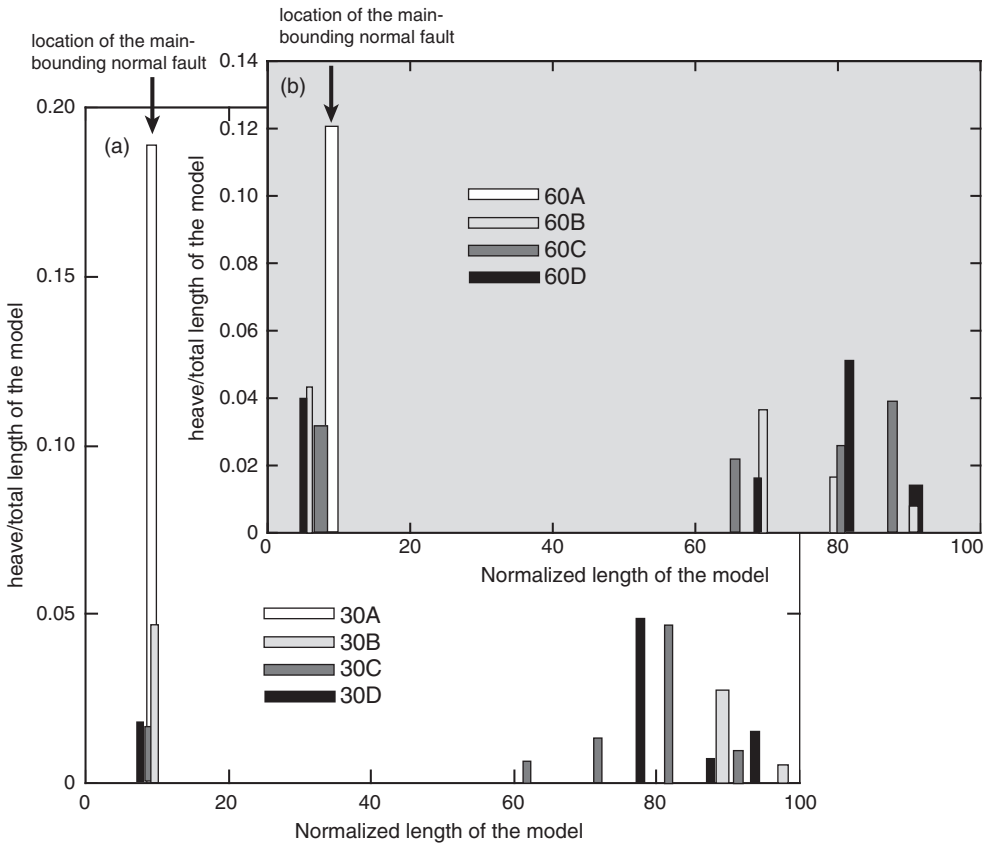

Fig. 8. Graphs illustrating the horizontal-extension accommodated by structures (on *y*) in relation with their across-strike position in the model (on *x*) in models (a) with 30° and (b) 60° of dip angle of the main-bounding normal fault.

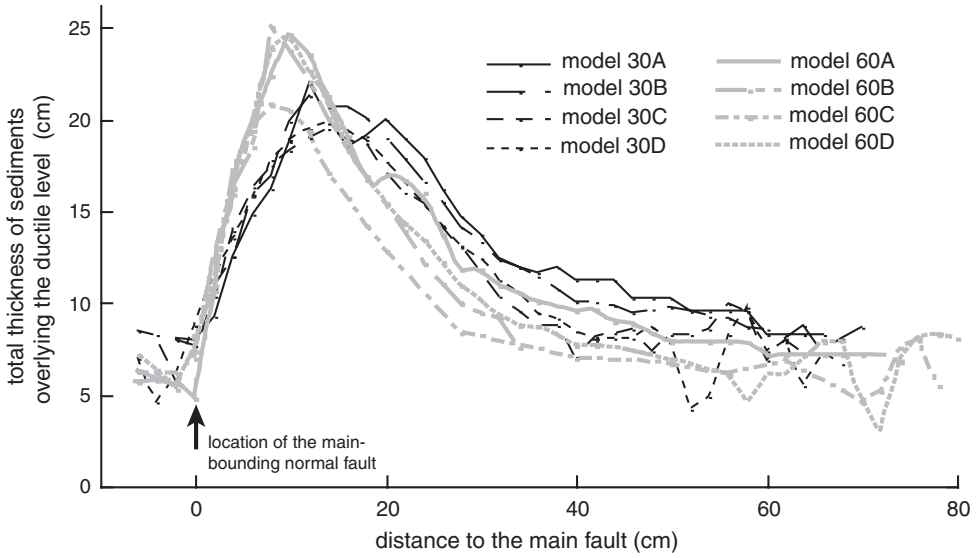

Fig. 9. Plot of total thickness of sediments overlying the interlayered viscous layer vs. the distance to the main-bounding normal fault in all models.

Sedimentary features

In all models, thickness variations in the syn-rift sequence are linked to slip of the main-bounding normal fault. The depocentre, elongated parallel to the main listric fault, is located over the hangingwall cut-off of the pre-rift sediments (Figs 2 and 3). The position and width of the depocentre vary with the dip of the master fault (Fig. 9). The depocentre is narrower and closer to the basin margin in models with a 60°-dipping fault. In all brittle–ductile

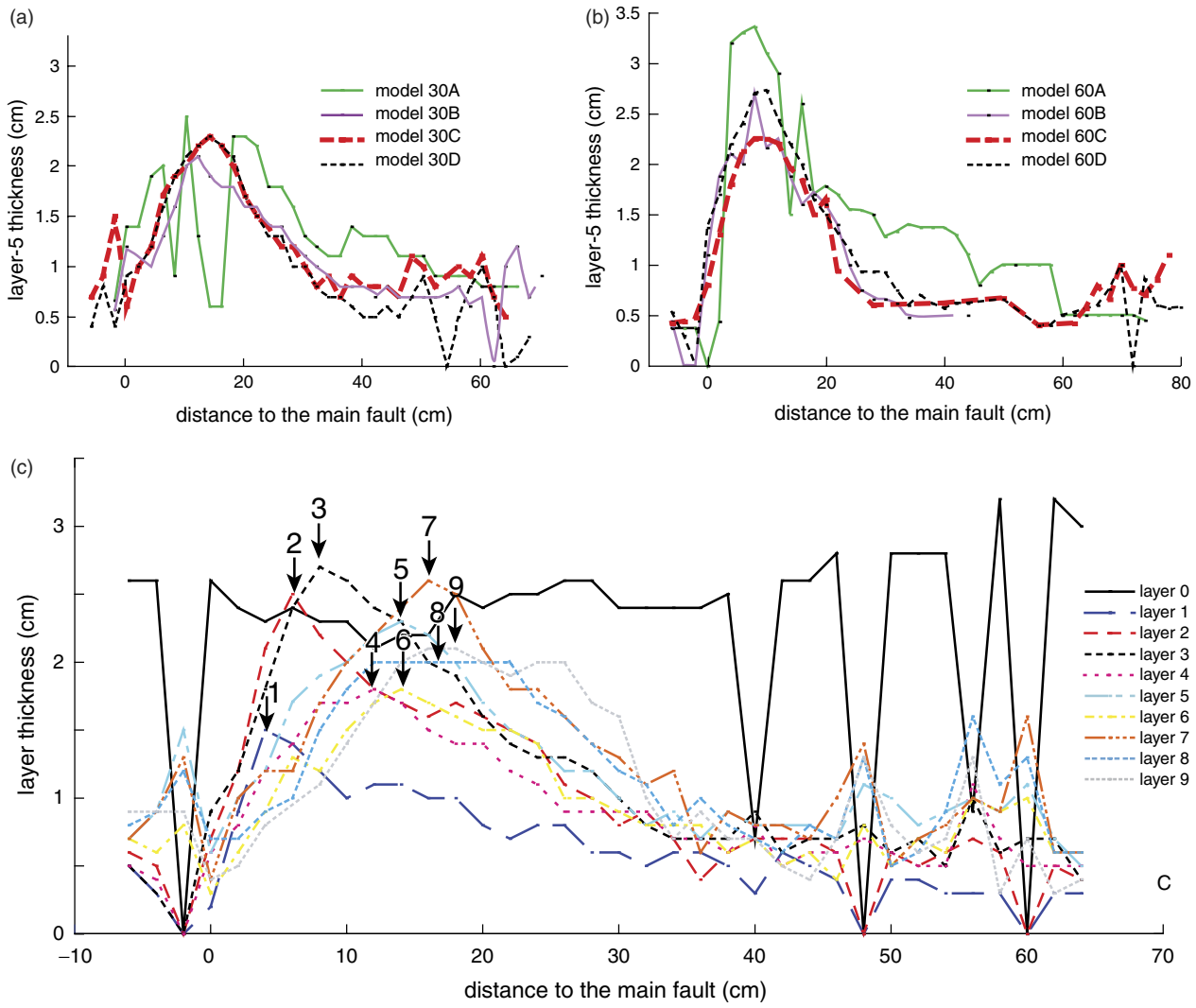

Fig. 10. (a, b) Plots illustrating the thickness of layer 5 of the syn-rift deposits vs. the distance to the main-bounding normal fault in all models. (c) Plot of the thickness of each syn-rift layer vs. the distance to the main-bounding normal fault in model 30C.

models, thickness variations are gradual in the growth syncline over the master fault. The thickness of the syn-rift deposits changes more abruptly near the pinch-out of the viscous layer in the opposite side of the model (Fig. 9).

To compare all models in detail, we measured the thickness of an intermediate syn-rift layer (layer 5) with respect to the distance to the main fault (Fig. 10a and b). The curves from brittle models show a saw-tooth shape, stronger in model 30A. In brittle–ductile models, these curves are smoother with increasing thickness of the ductile level (Fig. 10a and b). Similar to Fig. 9, the curves for models with a 60° dip angle of the master fault present a narrower and slightly higher maximum.

A quantitative analysis to study the sedimentary evolution of model 30C was undertaken by plotting the thickness of every layer against the distance to the main fault (Fig. 10c). This graph shows that the depocentre migrated progressively towards the basin centre. The older syn-rift layers show four minima at the opposite margin of the master fault (layers 0, 1 and 2) and a minimum at the footwall-margin of the basin (layers 0, 1, 2 and 3), coinciding with the relative maxima of the shallower layers. Three of the minima represent null sedimentation of the older syn-rift layers and all of them are associated with the occurrence of salt walls, grabens and half-grabens (Fig. 3).

The sedimentary architecture of the basin varies depending on the geometry of the master fault and thickness changes of the viscous layer (Figs 2 and 3). The 3D graphs of Appendix A represent a quantitative approach to describe the sedimentary architecture of all models. We divided models into five sectors and calculated the average dip angle of beds (on the abscise axis) and area (on the ordinate axis) for each sector (see Appendix A). Sand pack models (30A and 60A) show a different behaviour, whereas the general trend of brittle–ductile models is similar.

DISCUSSION

Comparison with previous works

In the last decades, extensional fault systems in the brittle crust have been intensively studied using analogue model-

ling. In general, three different model configurations have been used: (i) Type 1. Brittle models analysing the hangingwall deformation over a major sole listric fault with different geometries using a rigid footwall block (e.g. McClay & Ellis, 1987a, b; Ellis & McClay, 1988; McClay, 1990), (ii) Type 2. Brittle–ductile models to analyse the overburden deformation above an active master normal fault or basal discontinuity (e.g. Withjack *et al.*, 1990; Koyi *et al.*, 1993; Nalpas & Brun, 1993; Withjack & Callaway, 2000) and (iii) Type 3. Brittle–ductile models with uniform extension using a rubber sheet as a basal detachment (e.g. Brun & Choukroune, 1983; Vendeville *et al.*, 1987; McClay, 1990). The interplay of syn-rift sedimentation and deformation has been studied in the three types of experiments. However, only Types 2 and 3 have dealt with brittle–ductile models (i.e. sand–silicone) to analyse the influence of a viscous layer, a common feature in many sedimentary basins. In the present work, simple brittle–ductile models have an interlayered decóllement and a main-bounding listric fault (Type 1). The experimental results confirm that the occurrence of a viscous layer within the pre-rift sequence substantially modifies the sedimentary architecture of basins.

In experiment 30A, a brittle model where the master listric fault dips 30°, the geometry of the syn-rift deposits differs largely from model 60A or models presented by Ellis & McClay (1988), where the less steep experiment shows a 45° dip angle of the master fault. This is probably related to the friction angle of sand, which induces the formation of new normal faults with steeper dips than the shallow-dipping main normal fault to accommodate extension in the hangingwall of our model. This suggests that a threshold controls the geometry of sedimentary basins without interlayered décollements, whose value is directly controlled by the strength of the deposits and the dip of the master listric fault. Thus, the value of the internal friction angle of the sand in purely brittle models must be this threshold for the dip of the master listric fault.

Sedimentary differences related to an interlayered decóllement

The most common hangingwall structure formed during crustal extension is the roll-over anticline (e.g. Shelton, 1984; Poblet & Bulnes, 2005). The pre-rift sequence in all experiments defines a roll-over anticline, whereas syn-sedimentary roll-over anticlines only appear in some models when an interlayered decóllement is present. The syn-rift deposits of all brittle–ductile models defined a growth syncline, with dips progressively shallowing from the bottom to the top of the pre-rift sequence. Without a viscous layer, a complex listric fault, with a ramp-flat-type geometry, is required for hangingwall synclines (see Ellis & McClay, 1988).

Without the viscous layer, most deformation in the syn-rift sequence is close to the master normal fault, whereas with a viscous layer, deformation is more widely distributed because the viscous layer partly decouples deformation above and below it (Fig. 4). Withjack & Callaway (2000) also described this feature in brittle–ductile experiments analysing deformation in the cover deposits above an active normal fault. In our brittle–ductile models, a fault system at the opposite margin of the sedimentary basin develops (Figs 3 and 7). The origin of this fault system lies on the concentration of extensional stress at the termination of the ductile level. Distal grabens were also described by Withjack & Callaway (2000) in their models with a thick viscous layer. This phenomenon also occurs in compressional scenarios, where a rapid localization of the deformation front takes place along the outer boundary of the viscous décollement material (see Storti *et al.*, 2007).

Experimental limitations

Our analogue models include some oversimplifications with respect to natural sedimentary basins related to half-graben scenarios. (1) Rarely the boundary in half-grabens coincides with a sole main fault as in our models, instead of a system of faults. (2) In the experiments, the footwall block is rigid and non-deformable and the contrast of different rheologies between the hangingwall and footwall blocks is constant with extension. Also, the sand/silicone density ratio is higher than in nature, assuming a siliciclastic overburden above halite. (3) Variations in both the thickness of the viscous detachment level and the presence of secondary detachment levels, which were not included in our experiments, are, in fact, common in nature. (4) Syn-tectonic sedimentation at regular intervals, without erosion in the footwall block, is an ideal situation simulated in the laboratory; in nature, interruptions of sedimentation and even periods of erosion are common. (5) Our experimental programme consists of a two-dimensional (2D) analysis at a constant displacement rate, as we did not introduce along-strike variations or changes in the displacement rate. However, despite these experimental limitations our experimental set-ups are well suited to compare the different geometries obtained with and without detachment levels, and the qualitative variations occurring with different thickness of the detachment level and basin-bounding fault geometries.

APPLICATION TO NATURAL EXAMPLES

Partly and non-inverted extensional basins

Of the many well-studied extensional basins, especially within the Atlantic continental margins, the geometry of some of them can be explained by our experiments. Extensional basins with growth syncline geometry are linked either to shallow detachments within the pre-rift sequence or to systems of normal faults defining a graben instead of a single fault at the basin margin. One of the best case studies is the Jeanne d'Arc basin in the Terra Nova offshore, where evaporitic deposition occurred between the Late Triassic and Early Jurassic (Holser *et al.*, 1988) (Fig. 11a). Its syncline geometry has been interpreted as the result of

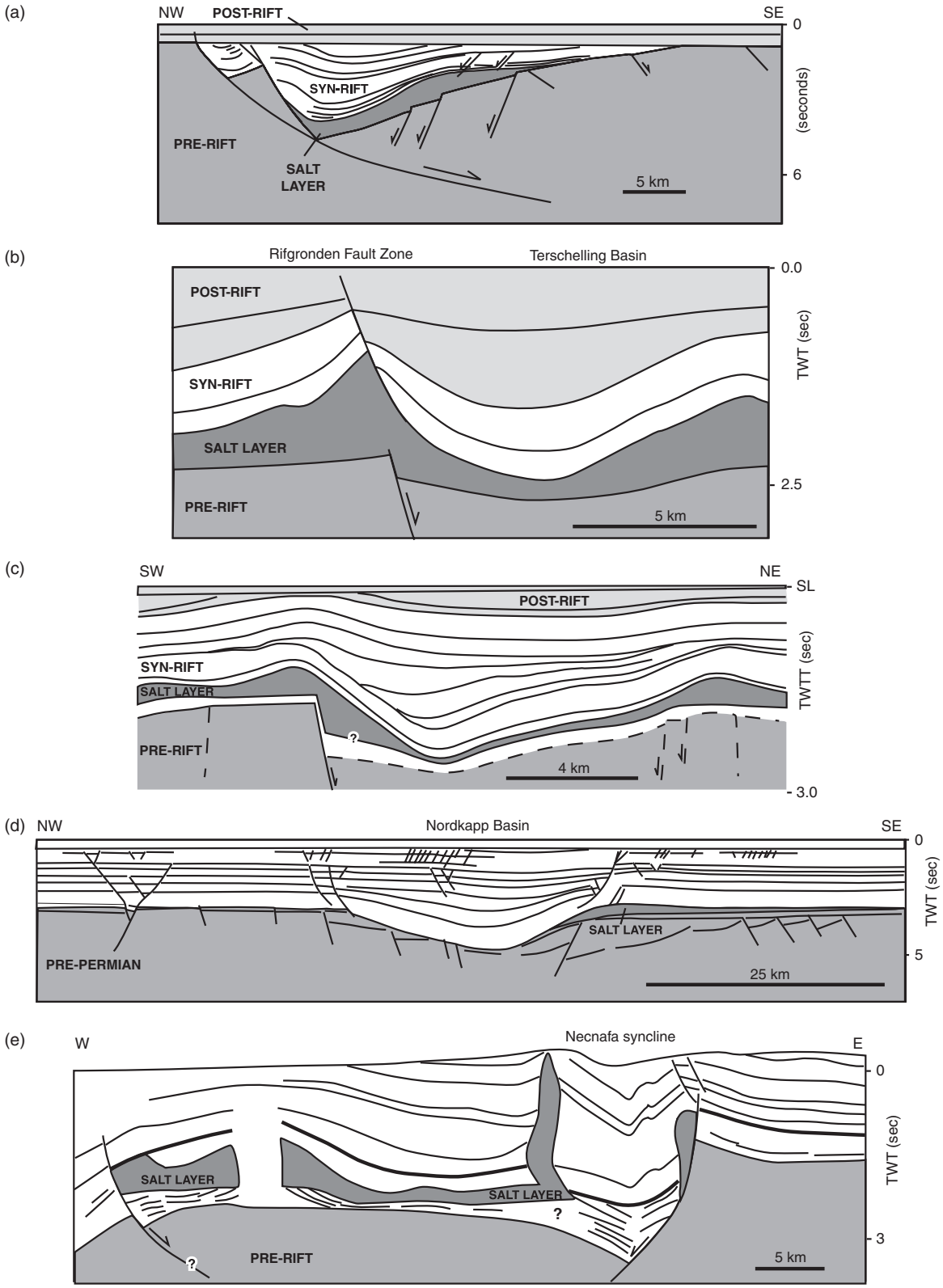

Fig. 11. (a) Southern Jeanne d'Arc basin, offshore Newfoundland. Sketch based on time-migrated seismic section 85-4A. Modified from Withjack & Callaway (2000). (b) Terschelling basin, Southern North Sea. Sketch based on seismic section SNST83-4. Modified from Remmelts (1995). (c) Northern Lusitanian basin, offshore Portugal. Sketch based on seismic line S84-23. Modified from Alves *et al.* (2002). (d) Nordkapp basin and Norsel high, southwestern Barents Sea. Interpreted seismic profile 11 modified from Gudlaugsson *et al.* (1998). (e) Essaouira basin, western Atlas system (Morocco). Sketch based on seismic profile, modified from Hafid (2000).

ramp–flat basement fault geometry (Tankard *et al*., 1989; McClay, 1990). However, our experimental results indicate that growth synclines can also develop linked to half-grabens containing a mid-level viscous décollement. Other features characterizing the Jeanne d'Arc basin that match well with our experimental results are (Fig. 11a): (1) the formation of a secondary roll-over anticline within the syn-rift sequence near the master fault. The origin of this structure linked to salt tectonics was also proposed by Withjack & Callaway (2000), and (2) the presence of subsalt faults affecting the pre-rift series that do not propagate upward.

The Mesozoic North Sea rift system also represents a good example with numerous 2D seismic sections published in the literature. In this case, the Upper Permian Zechstein salt constitutes the mid-level viscous décollement located in the upper part of the pre-rift series. Numerous works have dealt with salt tectonics evolving to this level (e.g. Coward & Stewart, 1995; Remmelts, 1995; Withjack & Callaway, 2000). In the Terschelling basin, in Southern North Sea, fault-related salt tectonics have been described by Remmelts (1995) and numerous features related to its extensional stage coincide with those described in our analogue models (Fig. 11b): (1) the syn-rift deposits described a growth syncline that has been tightened later during the Tertiary compressive phase as the Cenozoic post-rift sediments indicate, (2) a salt wall appeared in the cover deposits near the footwall cut-off of the listric fault. This salt wall, as in most brittle–ductile models (see Figs 5 and 6), was associated with a synthetic normal fault with the master fault detached within the Zechstein level (i.e. viscous layer) and (3) thickening and thinning of the salt layer took place as in our experiments, confirming the occurrence of salt flow.

Related to the opening of the North Atlantic Ocean, the Lusitanian Basin, offshore Portugal, represents a series of Late Triassic–Early Cretaceous rift-related basins (e.g. Rasmussen *et al*., 1998) containing a mid-level décollement in the lower part of the syn-rift deposits (Fig. 11c). The latest Triassic–Hettangian evaporites (Dagorda Formation) constitute this décollement, which largely conditioned the syn-rift sedimentary evolution and geometry of the basin (e.g. Alves *et al*., 2002). The bowl-shaped basins given by growth synclines, the formation of salt walls over the footwall block near the main basin-margin faults and salt withdrawals in the hangingwall areas described by Alves *et al*. (2002) (see Fig. 11c) validate our experimental results. Alves *et al*. (2002) also point out that the thickness of the salt layer played a major role in the tectono-sedimentary evolution of the Northern Lusitanian basin as our analogue models indicate.

The Southwestern Barents Sea, in the north-west of Eurasia, also represents a well-known region with numerous works based on seismic reflection data and where salt structures have been described as related to large evaporite accumulations deposited during the Late Carboniferous–Early Permian (e.g. Koyi *et al*., 1995). Several basins formed during late Palaeozoic rifting in the southwestern Barents Sea that were influenced later by several deformational stages during the Mesozoic and Cenozoic (e.g. Ziegler, 1988). One of these basins is the Nordkapp basin (Fig. 11d), characterized by a half-graben geometry, numerous diapirs and marginal salt pillows (e.g. Koyi *et al*., 1995; Gudlaugsson *et al*., 1998). As Fig. 11d shows, the syncline shape of the basin and the accumulation of salt on the footwall block suggest a major influence of the salt layer on its evolution and geometry similar to our brittle–ductile experiments.

The last example is a partly inverted basin, where the experimental results can help to provide clues about its previous extensional geometry. The Essaouira basin, western Atlas system (Morocco), consists of several Late Triassic–Early Liassic half-grabens, with continued minor tectonic activity during Jurassic and Cretaceous and later compressed from the end of Late Cretaceous onwards (e.g. Hafid, 2000). Salt diapirism and salt withdrawal processes have been described to be linked to the occurrence of Lower Jurassic evaporites that consist mostly of halite (Hafid, 2000). Thus, the Necnafa syncline has been interpreted as Jurassic to lower Cretaceous salt withdrawal (see Hafid, 2000) (Fig. 11e). According to our experiments, this syncline basin geometry could represent a growth structure associated with the activity of a major basement listric fault in a half-graben scenario and the presence of a mid-level viscous décollement. All these features are compatible with the characteristics found in the Essaouira basin (Fig. 11e), validating our experimental results and testing the influence of interlayered salt deposits on the syn-rift sedimentary evolution there.

Strongly inverted extensional basins: the Cameros basin (North Spain)

The potential application of the experiments shown in this paper can be extended to completely inverted basins when it is possible to infer their pre-inverted geometry. Also, this work can help to constrain the extensional geometry of an inverted basin and to understand salt tectonics related to their extensional stage when it is difficult to deduce its pre-inverted geometry.

The Cameros basin is a well-known Mesozoic basin extensively studied in the past decades (e.g. Casas Sainz, 1992; Guimerà *et al*., 1995; Casas-Sainz & Gil-Imaz, 1998; Mata *et al*., 2001). It is located in the north-west termination of the Iberian Chain, an intraplate mountain range in northern Spain (Fig. 12). Exceptionally well-preserved syn-extensional sediments in the hangingwall of the main thrust, geophysical data revealing its sedimentary Mesozoic geometry and the presence of the Upper Triassic evaporites at the upper part of the pre-rift sequence make the Cameros basin ideal for comparing and validating our experimental results and to make inferences on the imprint of a shallow interlayered décollement on the geometry of completely inverted sedimentary basins. The Cameros basin formed extensionally during the Late Jurassic–Early Cretaceous and was inverted during the Tertiary (e.g. Salas

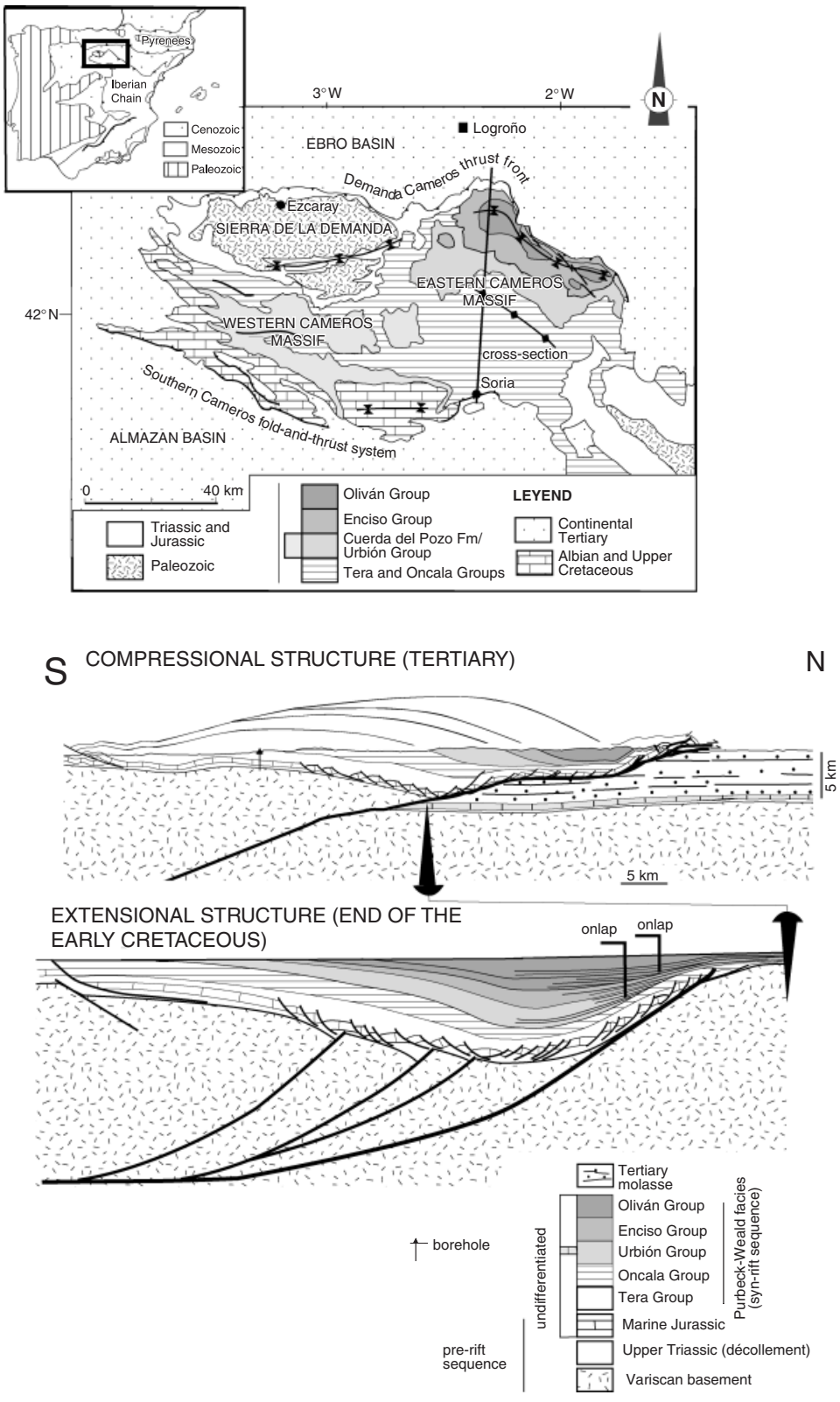

Fig. 12. Geological sketch, cross-section and reconstruction of the Cameros basin, showing its main features. Modified from Casas-Sainz & Gil-Imaz (1998), Mata *et al.* (2001) and Villalaín *et al.* (2003).

& Casas, 1993; Guimerà *et al.*, 1995). Its principal structures are located on its northern margin following the shape of its northern pre-inversion margin (e.g. Tischer, 1966; Guiraud, 1983; Guimerà *et al.*, 1995; Casas-Sainz & Gil-Imaz, 1998). Palaeozoic rocks and Triassic and Early Jurassic deposits constitute the pre-rift sequence in the Cameros basin. Among these, the Late Triassic Keuper evaporites form a well-known regional décollement (e.g. Guimerà & Álvaro, 1990). The syn-extensional deposits reach a preserved thickness of about 7000 m, thinning gently towards the South and more abruptly towards the North (e.g. Mata *et al.*, 2001). They consist of continental

rocks sedimented between the Kimmeridgian and the Albian (Muñoz *et al*., 1997). The syn-sedimentary structures of the basin have been reconstructed by means of thermal modelling (using fluid inclusions) (Mata *et al*., 2001) and palaeomagnetic analysis (Villalaín *et al*., 2003). According to these reconstructions, the main syn-extensional structure is a 100 km long, continuous basement-involved growth syncline linked to the movement of a major southward-dipping normal fault limiting the basin to the North. Large outcrops of Triassic gypsum in the northern basin margin (at present a north-directed thrust) point to an initially thick detachment. The southern part of the basin is characterized by listric normal faults with sharp changes in the thickness of the syn-rift deposits (Guimerà *et al*., 1995). Although many of these faults have been interpreted to be basement-involved faults (Guimerà *et al*., 1995), the vicinity of the pinch-out for the detachment level (Casas-Sainz *et al*., 2000) suggests that they can be detached within the Middle-Upper Triassic décollement, according to our experimental results.

In summary, many of the tectonic and sedimentary features converging in the Cameros basin are consistent with an extensional basin formed over a shallow décollement overlying a basement fault, and overlain by a thin section (between 500 and 800 m thick, Casas Sainz, 1992) of pre-rift rocks. Basinward dips of the syn-rift sequence (Villalaín *et al*., 2003) indicate a basement fault with intermediate dips between the end-members described in our experiments. Secondary structures described in the northern border of the Cameros basin, as roll-over anticlines (Casas-Sainz & Gil-Imaz, 1998), also fit with some of the features of the described models. Moreover, the experimental models presented can help to solve one of the main controversial topics about the formation of the basin: the presence of the pre-rift sequence throughout the northern basin border can be explained by diffuse extension by means of minor normal faults. The geometry of the younger syn-rift deposits (Urbión, Enciso and Oliván Groups) agrees with the half-graben geometry of our brittle–ductile models (Fig. 12). For the older syn-rift deposits (Tera and Oncala Groups), however, the depocentre of the Cameros basin was located southwards of the depocentre for the younger units. This suggests that different master faults have acted through time in the Cameros basin from South to North, contrasting with our experiments where only one major fault acts continuously.

CONCLUSIONS

Our experimental results of extension above a listric normal fault with a shallow viscous detachment layer within the pre-rift sequence indicate that the main structure formed within the syn-rift sediments is a growth syncline. As the basin evolved, the depocentre for each sedimentary unit migrates basinwards, as the hangingwall translates away from the master fault. An important shallow extensional system, with listric normal faults causing sharp thickness changes in the syn-rift sequence, forms near the pinch-out of the ductile level in the basin margin opposite to the main basement fault. This secondary fault system is more important with shallow dips of the main fault and with thicker viscous layers. Secondary structures, as small roll-over anticlines described by the syn-rift deposits near the bounding fault and salt walls near the footwall cut-off of the listric fault, appear linked to the movement of the main basement fault. The results indicate that growth synclines may be common in extensional environments, provided that a shallow décollement occurs within the pre-rift stratigraphic sequence and partly decouples strain above and below it. The comparison with several basin examples containing a mid-level décollement validates the experimental results and constrains their interpretations.

ACKNOWLEDGEMENTS

Models were constructed at the Analogue Modelling Laboratory of the University of Zaragoza (Spain). This work was supported by the projects BTE2002-04168 of the Dirección General de Enseñanza Superior (DGES), Spanish Ministry of Education, and BU002B06 of the Junta de Castilla y León. Financial support was also given by a predoctoral grant (Spanish Ministry of Education) to P. del Río and a *research position* for young scientists from the Spanish Ministry of Education and Science to R. Soto ('Juan de la Cierva' programme). Sylvia Gracia helped us in the laboratory works. We are very grateful to J. Cartwright and M. Jackson for helpful reviews that greatly improved the manuscript.

REFERENCES

Alves, T.M., Gawthorpe, R.L., Hunt, D.W. & Monteiro, J.H. (2002) Jurassic tectono-sedimentary evolution of the Northern Lusitanian Basin (offshore Portugal). *Mar. Petrol. Geol.*, **19**, 727–754.

Bahroudi, A. & Koyi, H.A. (2004) Tectono-sedimentary framework of the Gachsaran formation in the Zagros foreland basin. *Mar. Petrol. Geol.*, **21**, 1295–1310.

Brun, J.P. & Choukroune, R. (1983) Normal faulting, block tilting and décollement in a stretched crust. *Tectonics*, **2**, 345–356.

Buchanan, P.G. & McClay, K.R. (1991) Sandbox experiments of inverted listric and planar fault systems. *Tectonophysics*, **188**, 97–115.

Cartwright, J., Stewart, S. & Clark, J. (2001) Salt dissolution and salt-related deformation of the Forth Approaches Basin, UK North Sea. *Mar. Petrol. Geol.*, **18**, 757–778.

Casas Sainz, A.M. (1992) El frente norte de las Sierras de Cameros: estructuras cabalgantes y campo de esfuerzos, Tesis Doctoral, Instituto de Estudios Riojanos, Logroño.

Casas-Sainz, A.M., Cortés-Gracia, A.L. & Maestro-González, A. (2000) Intraplate deformation and basin formation during the Tertiary within the northern Iberian plate: origin and evolution of the Almazán Basin. *Tectonics*, **19**(2), 258–289.

Casas-Sainz, A.M. & Gil-Imaz, A. (1998) Extensional subsidence, contractional folding and thrust inversion of the Eastern Cameros Massif, northern Spain. *Geol. Rundsch.*, **86**, 802–818.

Clark, J.A., Stewart, S.A. & Cartwright, J.A. (1998) Evolution of the NW margin of the North Permian Basin, UK North Sea. *J. Geol. Soc. Lond.*, **155**(4), 663–676.

Costa, E. & Vendeville, B.C. (2002) Experimental insights on the geometry and kinematics of fold-and-thrust belts above weak, viscous evaporitic décollement. *J. Struct. Geol.*, **24**, 1729–1739.

Coward, M. & Stewart, S. (1995) Salt-influenced structures in the Mesozoic–Tertiary cover of the southern North Sea, U.K. In: *Salt Tectonics: A Global Perspective* (Ed. by M.P.A. Jackson, D.G. Roberts & S. Snelson), *AAPG Mem.,* **65**, 229–250.

Ellis, P.G. & McClay, K.R. (1988) Listric extensional fault systems-results of analogue model experiments. *Basin Res.*, **1**, 55–70.

Ge, H., Jackson, M.P.A. & Vendeville, B.C. (1997) Kinematics and dynamics of salt tectonics driven by progradation. *AAPG Bull.*, **81**, 398–423.

Gudlaugsson, S.T., Faleide, J.I., Johansen, S.E. & Breivik, A.J. (1998) Late Palaeozoic structural development of the South-western Barents Sea. *Mar. Petrol. Geol.*, **15**, 73–102.

Guimerà, J. & Álvaro, M. (1990) Structure et evolution de la compression alpine dans la Chaîne Ibérique et la Chaîne côtière catalane (Espagne). *Bull. Soc. Geol. France*, **VI**(2), 339–348.

Guimerà, J., Alonso, A. & Mas, J.R. (1995) Inversion of an extensional-ramp basin by a newly formed thrust: the Cameros basin (N Spain). In: *Basin Inversion* (Ed. by J.G. Buchanan & P.G. Buchanan), *Geol. Soc. London Spec. Publ.*, **88**, 433–453.

Guiraud, M. (1983) Evolution tectono sédimentaire du bassin wealdien (Crétacé inferieur) en relais de décrochement de Logroño-Soria (NW Espagne). III Cycle Thesis. University of Montpellier.

Hafid, M. (2000) Triassic–early Jurassic extensional systems and their Tertiary inversion, Essaouira basin (Morocco). *Mar. Petrol. Geol.*, **17**, 409–429.

Holser, W.T., Clement, G.P., Jansa, L.F. & Wade, J.A. (1988) Evaporite deposits of the North Atlantic rift. In: *Triassic–Jurassic Rifting, Continental Breakup and the Origin of the Atlantic Ocean and Passive Margins* (Ed. by W. Manspeizer), *Dev. Geotecton.,* **22**, 525–556.

Koyi, H., Jenyon, M.K. & Petersen, K. (1993) The effect of basement faulting on diapirism. *J. Petrol. Geol.*, **16**, 285–312.

Koyi, H., Talbot, C.J. & Tørudbakken, B.O. (1995) Salt tectonics in the Northeastern Nordkapp basin, Southwestern Barents sea. In: *Salt Tectonics: A Global Perspective* (Ed. by M.P.A. Jackson, D.G. Roberts & S. Snelson), *AAPG Mem.,* **65**, 437–448.

Luján, M., Storti, F., Balanyá, J.C., Crespo-Blanc, A. & Rosetti, F. (2003) Role of décollement material with different rheological properties in the structure of the Aljibe thrust imbricate (Flysch Trough, Gibraltar Arc): an analogue modelling approach. *J. Struct. Geol.*, **25**(6), 867–881.

Mata, M.P., Casas, A., Canals, A., Gil, A. & Pocoví, A. (2001) Thermal history during Mesozoic extension and Tertiary uplift in the Cameros Basin, northern Spain. *Basin Res.*, **13**, 1–22.

McClay, K.R. (1989) Analogue models of inversion tectonics. In: *Inversion Tectonics* (Ed. by M.A. Cooper & G.D. Williams), *Geol. Soc. London Spec. Publ.*, **44**, 41–59.

McClay, K.R. (1990) Physical models of structural styles during extension. In: *Extensional Tectonics and Stratigraphy of the North Atlantic Margins* (Ed. by A.J. Tankard & H.R. Balkwill), *AAPG Mem.,* **46**, 95–110.

McClay, K.R. & Ellis, P.G. (1987a) Analogue models of extensional fault geometries. In: *Continental Extensional Tectonics* (Ed. by M.P. Coward, J.F. Dewey & P.L. Hancock), *Geol. Soc. London Spec. Publ.*, **28**, 109–125.

McClay, K.R. & Ellis, P.G. (1987b) Geometries of extensional fault systems developed in model experiments. *Geology,* **15**, 341–344.

Muñoz, A., Soria, A.R., Canudo, J.I., Casas, A.M., Gil, A. & Mata, M.P. (1997) Caracterización estratigráfica y sedimentológica del Albiense marino del borde Norte de la Sierra de Cameros. Implicaciones paleogeográficas. *Cuad. Geol. Ibér.*, **22**, 139–163.

Nalpas, T. & Brun, J.P. (1993) Salt flow and diapirism related to extension at crustal scale. *Tectonophysics*, **228**, 349–362.

Phillippe, Y., Deville, E. & Mascle, A. (1998) Thin-skinned inversion tectonics at oblique basin margins: example of the western Vercors and Chartreuse Subalpine massifs (SE France). In: *Cenozoic Foreland Basins of Western Europe* (Ed. by A. Mascle, C. Puigdefábregas, H.P. Luterbacher & M. Fernández), *Geol. Soc. London Spec. Publ.*, **134**, 1–28.

Poblet, J. & Bulnes, M. (2005) Fault-slip, bed-length and area variations in experimental rollover anticlines over listric normal faults: influence in extension and depth to detachment estimations. *Tectonophysics*, **396**, 97–117.

Rank-Friend, M. & Elders, C.F. (2004) The evolution and growth of Central Graben salt structures, Salt Dome Povince, Danish North Sea. In: *3D Seismic Technology: Application to the Exploration of Sedimentary Basins* (Ed. by R. Davies, J.A. Cartwright, S.A. Stewart, M. Lappin & J.R. Underhill), *Mem. Geol. Soc. Lond.,* **29**, 149–163.

Rasmussen, E.S., Lomholt, S., Andersen, C. & Vejbæk, O.V. (1998) Aspects of the structural evolution of the Lusitanian Basin in Portugal and the shelf and slope area offshore Portugal. *Tectonophysics*, **300**, 199–255.

Remmelts, G. (1995) Fault-related salt tectonics in the Southern North Sea, the Netherlands. In: *Salt Tectonics: A Global Perspective* (Ed. by M.P.A. Jackson, D.G. Roberts & S. Snelson), *AAPG Mem.,* **65**, 261–272.

Richard, P. (1991) Experiments on faulting in a two-layer cover sequence overlying a reactivated basement fault with oblique-slip. *J. Struct. Geol.*, **13**, 459–469.

Rodríguez-López, J.P., Liesa, C.L., Meléndez, N. & Soria, A.R. (in press) Normal fault development in a sedimentary succession with multiple detachment levels: the Lower Cretaceous Oliete sub-basin, Eastern Spain. *Basin Research*, doi: 10.1111/j.1365-2117.2007.00327.x.

Salas, R. & Casas, A. (1993) Mesozoic extensional tectonics, stratigraphy and crustal evolution during the Alpine cycle of the eastern Iberian basin. *Tectonophysics*, **228**, 33–35.

Sans, M. & Koyi, H.A. (2001) Modeling the role of erosion in diapir development in contractional settings. *Geol. Soc. Am. Mem.*, **193**, 111–121.

Shelton, J.W. (1984) Listric normal faults: an illustrated summary. *AAPG Bull.*, **68**, 801–815.

Storti, F., Soto Marín, R., Rossetti, F. & Casas Sainz, A.M. (2007) Evolution of experimental thrust wedges accreted from along-strike tapered, silicone-floored multilayers. *J. Geol. Soc. Lond.*, **164**, 73–85.

Tankard, A.J., Weilsink, H.J. & Jenkins, W.A.M. (1989) Structural analysis and stratigraphy of the Jeanne d'Arc Basin, Grand Banks of Newfoundland. In: *Extensional Tectonics and Stratigra-*

phy of the North Atlantic Margins (Ed. by A.J. Tankard & H.R. Balkwill), *AAPG Mem.*, **46**, 265–282.

Tischer, G. (1966) El delta Weáldico de las montañas Ibéricas Occidentales y sus enlaces tectónicos. *Notas Comun. Inst. Geol. Min. España*, **81**, 53–78.

Ustaszewski, K., Schumacher, M., Schmid, S.M. & Nieuwland, D. (2005) Fault reactivation in brittle-viscous wrench systems–dynamically scaled analogue models and application to the Rhine–Bresse transfer zone. *Quat. Sci. Rev.*, **24**, 365–382.

Vendeville, B., Hongxing, G. & Jackson, M.P.A. (1995) Scale models of salt tectonics during basement-involved extension. *Petrol. Geosci.*, **1**, 179–183.

Vendeville, B.C., Cobbold, P., Davy, P., Brun, J.P. & Choukroune, P. (1987) Physical models of extensional tectonics at various scales. In: *Continental Extensional Tectonics* (Ed. by M.P. Coward, J.F. Dewey & P.L. Hancock), *Geol. Soc. London Spec. Publ.*, **28**, 95–107.

Vendeville, B.C. & Jackson, M.P.A. (1992) The rise of diapirs during thin-skinned extension. *Mar. Petrol. Geol.*, **9**, 331–353.

Villalaín, J.J., Fernández-González, G., Casas, A.M. & Gil-Imaz, A. (2003) Evidence of a Cretaceous remagnetization in the Cameros Basin (North Spain): implications for basin geometry. *Tectonophysics*, **377**, 101–117.

Weijermars, R. (1986) Flow behaviour and physical chemistry of bouncing putties and related polymers in view of tectonic laboratory applications. *Tectonophysics*, **124**, 325–358.

Withjack, M., Olson, J. & Peterson, E. (1990) Experimental models of extensional forced folds. *AAPG Bull.*, **74**, 1038–1054.

Withjack, M.O. & Callaway, S. (2000) Active normal faulting beneath a salt layer: an experimental study of deformation patterns in the cover sequence. *AAPG Bull.*, **84**(5), 627–251.

Ziegler, P.A. (1988) Evolution of the Arctic-North Atlantic and the Western Tethys. *Am. Assoc. Petrol. Geol. Mem.*, **43**, 198pp.

Manuscript received 16 August 2006; Manuscript accepted 29 May 2007.

APPENDIX A

3D graphs representing the average dip angle of beds (on *y*) and area (on *z*) for five sectors of all models (in the cross-section photograph).